Improved sky line cancellation for high-res observations of the 587.032 cm^{-1}/17μm H_2 S(1) line

A recurring issue with this kind of observation is non-cancellation of sky emission lines, which could overlap or distort the baseline around the true astrophysical emission. Because the target emission often extends to the edges of the 19" long slit, the usual methods to subtract a background region along the slit cannot be used.

We devised a method to remove the problematic residual emission by adding and subtracting small fractions of the sky radiance spectrum (the sky flux before nod-subtraction).

New versions of the 2-D spectral product "COA" files are provided here with the suffix "_residualcorrected" in their filenames. These have the same flux units and format as the standard IRSA version COA file.
The EXES Handbook for Archive Users provides guidance for extracting 1-D spectra from the 2-D COA files.

In three observations listed in Table 1, the residual correction was unneeded, but we include the unaltered COA file from the main IRSA archive for completeness. The observations that did not need residual correction were: 3c391, and NGC 7023 P1 and NGC 7023 P2.

We also provide 1-D extracted spectra for each observation. The format of these spectra is ASCII files with filenames containing <sourcename>_h2s1_f<flightnumber>.dat, and are in terms of vlsr (km s^{-1}) and mean intensity (Jy $arcsec^{-2}$). In 2 instances, IC 443C and IC 443 G, we combine multiple nights of observations, weighting by the integration times.

Table 1: EXES observations of the H_2 S(1) line

Target	RA/DEC (J2000)	Flight	AOR ID	Date	EXPTIME(s)	SLTW(″)	TELVPA(°)	V_{lsr} offset (km/s)
IC 443 B	6:17:16.1 +22:25:15	862	07_0007_32	2022-04-29	960	3.2	332.5-326.8	36.70
IC 443 C	6:17:42.37 +22:21:16.88	860	07_0007_34	2022-04-27	1344	3.2	328.9-322.1	37.30
IC 443 C	6:17:42.37 +22:21:16.88	861	07_0007_34	2022-04-28	720	3.2	320.4-315.9	37.03
IC 443 C	6:17:42.37 +22:21:16.88	862	07_0007_34	2022-04-29	624	3.2	323.4-321.0	36.74
IC 443 G	6:16:43.6 +22:32:37	860	07_0007_28	2022-04-27	384	3.2	317.9	37.20
IC 443 G	6:16:43.6 +22:32:37	861	07_0007_28	2022-04-28	768	3.2	326.1-322.7	36.92
3c391	18:49:22.56 -00:57:17.25	860	07_0007_36	2022-04-27	1152	3.2	269.3-274.9	-42.16
ρ Oph p1	16:25:54.25 -24:19:13.0	830	09_0211_1	2022-02-25	1104	2.11	262.0-264.7	-40.23
ρ Oph p2	16:25:52.0 -24:19:15.5	836	09_0211_11	2022-03-08	768	2.11	271.6-274.0	-39.92
NGC 7023 p1	21:02:09.0 +68:09:05.0	831	09_0211_5	2022-02-26	576	2.11	263.8-257.5	-7.13
NGC 7023 p2	21:02:07.5 +68:09:03.5	831	09_0211_13	2022-02-26	384	2.11	254.3-248.8	-7.13
DR 21	20:39:01.4 +42:23:53	836	09_0210_1	2022-03-08	1296	2.65	236.4-221.5	-20.84
DR 21	20:39:01.4 +42:23:53	837	09_0210_1	2022-03-09	1104	2.65	239.6-230.3	-21.11

Deriving a template from the SCO radiance spectrum

The 587 cm^{-1} region is only affected by atmospheric CO_2 and N_2O.

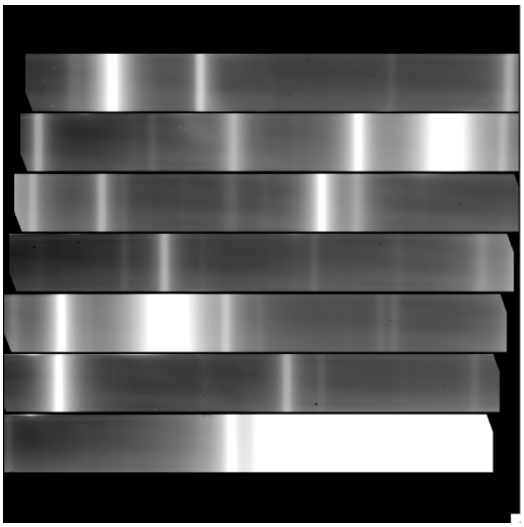

IC 443C sky radiance in "SCO" file.

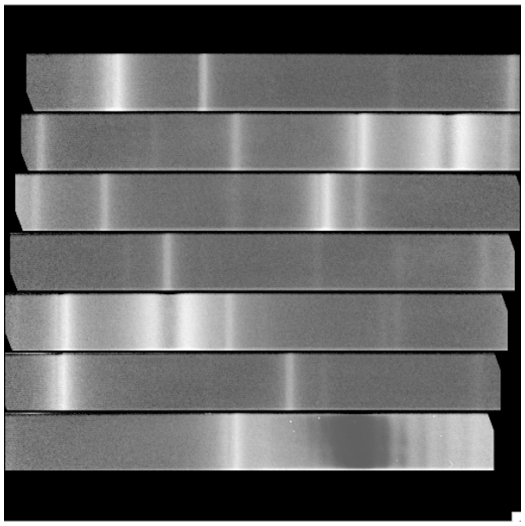

IC 443C nod subtracted file with telluric residuals.

In all H_2 S(1) observations there is only ever one order in the echellogram containing the 587cm^{-1} H2 emission line (even considering the various Doppler shifts to the different targets). Furthermore, only the right side of the order contains the 587cm-1 line (this order spans from 586.4-587.15cm-1), so at most, two atmospheric lines will contaminate the H2 emission.

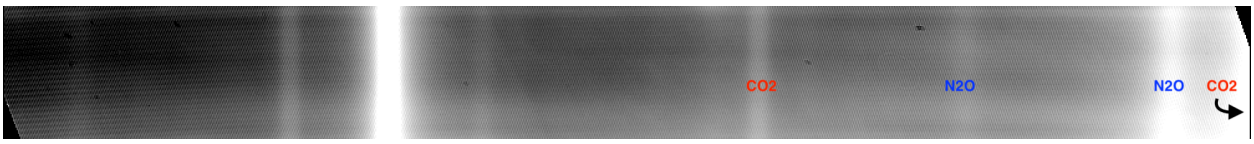

We separate the emission from the two problematic lines of N_2O and CO_2 from the SCO sky radiance, by making Gaussian fits to the N_2O lines in the SCO file. The remaining template contained CO_2, but also N_2O in the other orders and thermal telescope and sky emission, which cannot be separated from the telluric line emission.

The we add factors of about -/+ 0.005 x of the separate templates until the residuals away from the possible H_2 emission are eliminated.

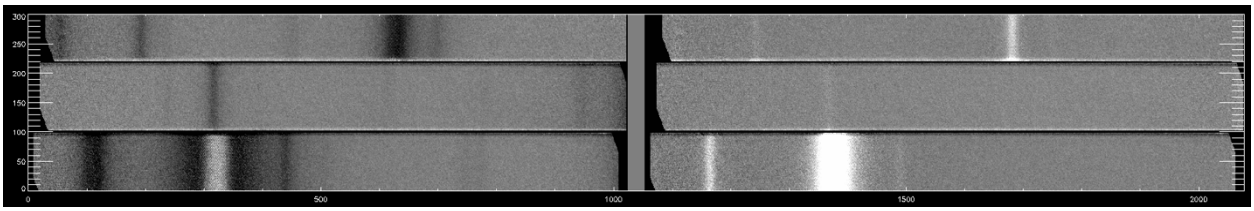

Figure 1 DR 21. Flight 837. Left panel: Strong residual lines before removal process. Right panel: Residuals after suppression. Note that strong lines in other orders are not well removed and actually turn to a positive residual, but the relatively weak residuals that affect our targeted H2 emission are nearly eliminated.

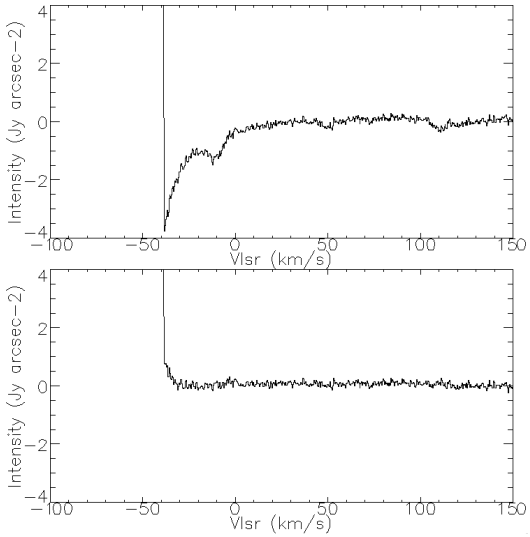

Figure 2 DR 21 Top panel (before). Bottom panel (after correction). The observation was a non-detection.

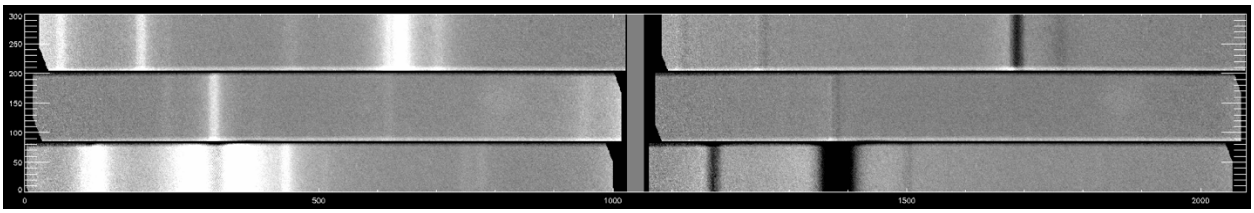

Figure 3 IC 443B. Left panel: Positive residual contaminate the S(1) line emission. (right panel): Residuals after suppression. Note that strong lines in adjacent orders were not completely removed, but the relatively weak residuals that affect our targeted H2 emission are nearly eliminated.

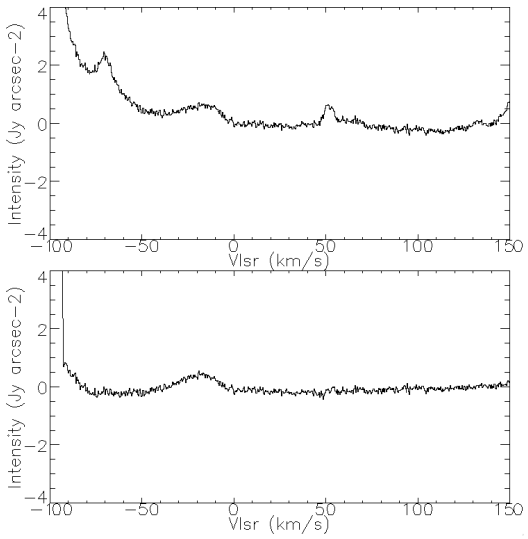

Figure 2 IC 443B top panel (before), bottom panel (after correction). The H_2 emission line is detected as the broad bump centered at vlsr=-20 km/s.

Secondly, we provided 1-D extractions of the H2 S(1) spectra. Only the relevant order with the S(1) line frequency is included.

Column 1 is the velocity channel, with respect to v_{lsr}.
Column 2 is the mean intensity of the inner 8" of the slit. This matches the extraction size of the H_2 S(5) 1447cm^{-1} observations in the IRSA archive, so it is the best match for comparison.
Column 3 is the mean intensity of the inner 16" of the slit. This is majority of the slit full length, 19", but avoids order edge flat fielding issues.
Column 3 in the transmission model.

```
# Intensity vs v_lsr, derived from
# file =F0862_EX_SPE_07000732_EXEELONEXEECHL_COA_40025-40029.fits
#########################
# Vlsr (km/s)    Intensity, 8 arcsec aperture (Jy arcsec-2)   Intensity,16 arcsec aperture (Jy arcsec-2)    transmission
         NaN             NaN             NaN         NaN
         NaN             NaN             NaN         NaN
         NaN             NaN             NaN         NaN
         NaN             NaN             NaN         NaN
         NaN             NaN             NaN         NaN
         NaN             NaN             NaN         NaN
         NaN             NaN             NaN         NaN
         NaN             NaN             NaN         NaN
         NaN             NaN             NaN         NaN
         NaN             NaN             NaN         NaN
         NaN             NaN             NaN         NaN
         NaN             NaN             NaN         NaN
         NaN             NaN             NaN         NaN
     272.977             NaN             NaN       0.995
     272.611             NaN             NaN       0.995
     272.245             NaN             NaN       0.995
     271.879             NaN             NaN       0.995
     271.513             NaN             NaN       0.995
     271.147           0.768           0.674       0.995
     270.781           0.555           0.617       0.995
     270.415           0.313           0.406       0.995
     270.050           0.572           0.489       0.995
     269.684           0.490           0.483       0.995
     269.318           0.480           0.574       0.995
     268.952           0.377           0.273       0.995
     268.586           0.579           0.447       0.995
     268.220           0.524           0.484       0.995
     267.854           0.429           0.621       0.995
     267.488           0.275           0.355       0.995
     267.122           0.621           0.444       0.995
     266.756           0.586           0.438       0.995
     266.390           0.422           0.374       0.995
     266.024           0.362           0.437       0.995
```

Figure 5: A part of the 1-D spectrum for IC 443B.